A Study on High Temperature Effects in Shock Wave/Boundary Layer Interaction Induced by Compression Corner

Matsumoto, Akira
Department of Aeronautics and Astronautics : Graduate Student

Aso, Shigeru
Department of Aeronautics and Astronautics : Professor

Kurotaki, Takuji
National Aerospace Laboratory : Japan : Senior Researcher

出版情報：九州大学工学紀要. 63 (2), pp.123-138, 2003-06-26. 九州大学大学院工学研究院
バージョン：
権利関係：

Memoirs of the Faculty of Engineering, Kyushu University, Vol. 63, No. 2, June 2003

A Study on High Temperature Effects in Shock Wave/Boundary Layer Interaction Induced by Compression Corner

by

Akira MATSUMOTO * , Shigeru ASO ** and Takuji KUROTAKI ***

(Received April 2, 2003)

Abstract

High temperature effects on shock wave-boundary layer interaction induced by two-dimensional compression corner have been numerically investigated. When a strong normal shock wave impinges on a ramp surface and reflects on the surface, steady flow is induced behind a normal shock wave and the flow separates near the compression corner and shock-wave/boundary-layer interaction region is formed. Since the static temperature of the flow is quite high enough for oxygen gas and nitrogen gas to dissociate, high temperature effects including dissociation and recombination of oxygen and nitrogen play very important roles in aerodynamic heating phenomena of shock-wave/boundary-layer interaction. The effects of chemical reactions on peak heating, peak pressure and separation length have been investigated. Also the effects of wall catalysis and free stream pressure to shock-wave/boundary-layer interaction flow fields are also discussed. The results show chemical reaction makes separation region smaller and surface catalytic effect is significant role to surface heating.

Keywords : Shock wave-boundary layer interaction, High temperature effects, CFD, Reusable launch vehicle

Nomenclature

*Graduate Student, Department of Aeronautics and Astronautics
**Professor, Department of Aeronautics and Astronautics
***Senior Researcher, National Aerospace Laboratory, Japan

E : total energy per unit volume [J/m^3]
D_s : effective diffusion coefficent of species s [m^2/s]
k_w : catalytic velocity
L : Length [m]
M_s : shock Mach number
p : pressure of mixture gas [Pa]
q : heat flux [W/m^2]
Re : Reynolds number [1]
T : temperature [K]
$\dot{w}_s$: mass production rate of species s [kg/sec]
u_i : velocity [m/sec]
$V_{s,i}$: diffusion velocity of species s in direction i [m/sec]
$\delta_{i,j}$: Kronecker's delta
θ_w : angle of a ramp surface [degrees]
ρ : density of mixture gas [kg/m^3]
ρ_s : density of species s [kg/m^3]
$\tau_{i,j}$: viscous stress tensor [N/m^2]

Subscripts

w : wall
s1 : primary separation point
s2 : secondary separation point
r1 : primary reattachment
r2 : secondary reattachment
p1 : local peak near primary reattachment point
p2 : local peak near secondary reattachment point
u : undisturbed

1. Introduction

Recently, International Space Station (ISS) is under construction at the Low Earth Orbit (LEO). The development of new type of space transportation systems is in progress in United States and European countries. The systems have to satisfy the strong demands for safety, credibility and low cost. Therefore, fundamental studies on fully reusable launch vehicles should be conducted. Fully reusable launch vehicles consist of many modules and they usually have complex configuration. Therefore, shock wave interference problems is essentially inevitable and important problem for the fully reusable launch vehicles. There are many types of shock wave interference problems around the fully reusable launch vehicle as shown in **Fig. 1**.

Especially it is very important to predict aerodynamic heating and peak pressure in the shock wave interaction region for the structural design. Moreover, those problems are very complicated including high temperature effects for the fully reusable launch vehicle which fly at higher Mach number. Here, high temperature effects are summarized as follows:

1. chemical reaction and chemical nonequilibrium
2. energy exchange among each internal energy modes and thermal nonequilibrium
3. emission and absorption of radiation

When the vehicles fly at high altitude and high Mach number, the flow around the vehicles are chemically and thermally non-equilibrium. In the flow characteristic time for energy exchange among each internal energy modes and chemical reaction become same order as that of a flow. Therefore, processes of chemical reaction and energy exchange can not be ignored. Additionally, radiation emitted from high temperature shock layer is enhanced, then unabsorbed radiation is transferred to body surface and causes radiative surface heating.

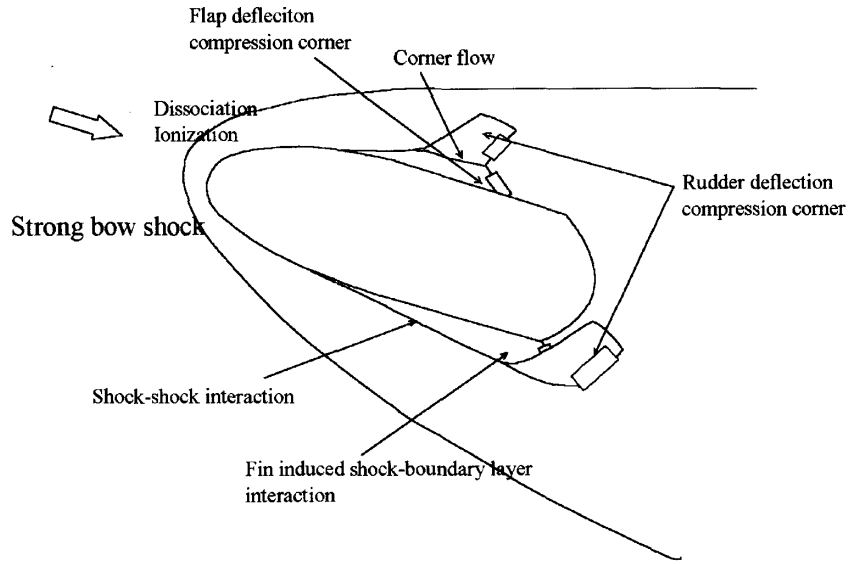

Fig. 1 Shock wave interference problems around a winged vehicle

Many researches have been investigating on shock interference problems[1-7]. However, aerodynamic heating phenomena including high temperature effects are not understood sufficiently. High temperature effects drastically affects to flowfield. Especially, dissociation and surface recombination play very important roles in a shock interference problems.

In the present paper, shock wave-boundary layer interaction with high temperature effects has been considered. Especially, two-dimensional compression corner flows are numerically investigated. Schematics of shock wave-boundary layer interaction near a two-dimensional compression corner with shock wave impingement to a ramp surface are shown in **Fig. 2**. A normal shock wave impinges on a ramp surface. Steady flow is induced behind a

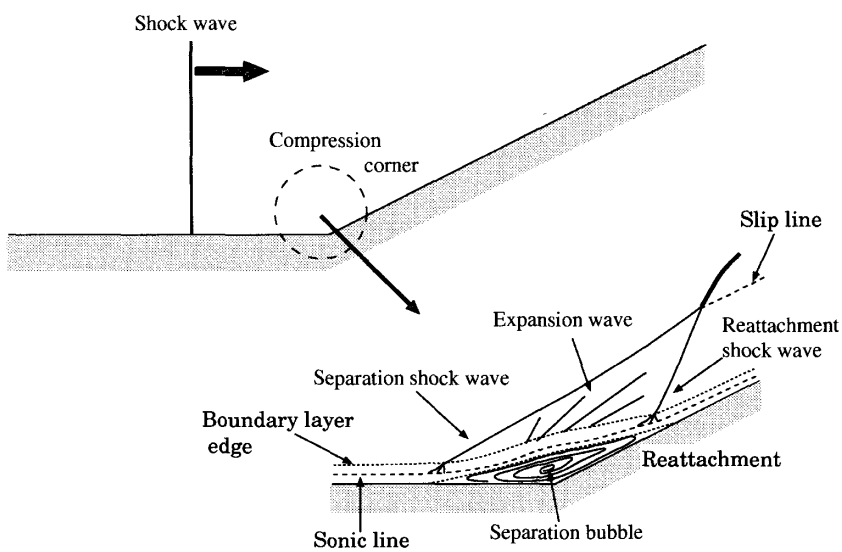

Fig. 2 Schematics of shock wave-boundary layer interaction near a two-dimensional compression corner

normal shock wave. The flow separates due to adverse pressure gradient at the compression corner. Then shock wave-boundary layer interaction region is formed near the compression

corner.

2. Numerical Method

2.1 Physical Models and Governing Equations

Dissociated air without ionization is considered as a test gas. Thus, N_2, O_2, N, O and NO are considered as dominant species. For the species, 17-reactions are considered. They are tabulated in **Table 1**. Each reaction rates are evaluated by Arrhenius's law importing

Table 1 Chemical reactions

r	Reactants		Products	M(Third Body)
1	O_2+M_1	$\rightleftharpoons$	$2O+M_1$	O, N, NO, O_2, N_2
2	N_2+M_2	$\rightleftharpoons$	$2N+M_2$	O, NO, O_2, N_2
3	N_2+N	$\rightleftharpoons$	$2N+N$	
4	$NO+M_3$	$\rightleftharpoons$	$N+O+M_3$	O, N, NO, O_2, N_2
5	NO+O	$\rightleftharpoons$	O_2+ N	
6	N_2+O	$\rightleftharpoons$	NO+N	

coefficients arranged by Blottner[8]. Transport properties are evaluated by small disturbance expansion based on Chapman-Enskog procedure. Procedures of Hirschfelder and Chapman-Cowling are adequately simplified by Yos[9,10]. The Yos' model is adapted in the present study. Diffusion velocity of each chemical species is evaluated considering mass diffusion only. They are also evaluated by small disturbance expansion proposed by Jones & Boris[11]. The first term of the expansion is taken then diffusion velocity is same expression as formulation of Curtiss & Hirchfelder[12].

Conservation equations for nonequilibrium high temperature flows around AOTV (Aeroassisted Orbital Transfer Vehicles) are derived from Boltzmann equation by Lee[13]. These equations are reformulated for one temperature description(thermal equilibrium) in the present study. Those equations are

- mass conservation equations for each chemical species
- global mass conservation equation
- momentum conservation equations
- total energy conservation equation

They are arranged as the full Navier-Stokes equations. In two-dimensional Cartesian coordinate, they are written in conservative, dimensional and tensor form[14];

$$\frac{\partial \boldsymbol{Q}}{\partial t} + \frac{\partial \boldsymbol{F}_k}{\partial x_k} = \frac{\partial \boldsymbol{F}_{vk}}{\partial x_k} + \boldsymbol{S} \tag{1}$$

$$\boldsymbol{Q} = \begin{bmatrix} \rho \\ \rho u_1 \\ \rho u_2 \\ E \\ \rho_1 \\ \vdots \\ \rho_{ns} \end{bmatrix}, \boldsymbol{F}_k = \begin{bmatrix} \rho u_k \\ \rho u_1 u_k + \delta_{1,k} p \\ \rho u_2 u_k + \delta_{2,k} p \\ (E+p)u_k \\ \rho_1 u_k \\ \vdots \\ \rho_{ns} u_k \end{bmatrix}, \boldsymbol{F}_{vk} = \begin{bmatrix} 0 \\ \tau_{k,1} \\ \tau_{k,2} \\ q_k + \tau_{k,1}u_1 + \tau_{k,2}u_2 \\ \rho_1 V_{1,k} \\ \vdots \\ \rho_{ns} V_{ns,k} \end{bmatrix}, \boldsymbol{S} = \begin{bmatrix} 0 \\ 0 \\ 0 \\ 0 \\ \dot{w}_1 \\ \vdots \\ \dot{w}_{ns} \end{bmatrix}$$

2.2 Numerical Schemes

Governing equations are extended to generalized coordinate system, and discretized by finite difference method. Vertex-centered method is applied in the present study. Therefore, independent variables are defined at each computational nodes. Strength of shock waves, expansion wave and contact discontinuities are quite large in hypersonic flows, therefore discritization scheme for convective terms is important to obtain adequately accurate solutions. In the present study, AUSM_DV[15] is applied to evaluate numerical flux for convective fluxes at each node-to-node points. The AUSM_DV is one of the most robust and efficient flux splitting scheme for hypersonic flow computations. MUSCL extrapolation[16,17] is applied for primitive variables($\tilde{\boldsymbol{q}} = [\rho, u, v, p, \rho_s]^T$) to construct Riemann problem in spatially second order. MINMOD(MINimum MODulous) limiter function is employed to satisfy TVD condition in MUSCL extrapolation procedure. Viscous fluxes are discretized in central difference manner based on Gauss' theorem. Temporally second order unsteady solutions are obtained by two-stage Runge-Kutta method[18] in the present study.

2.3 Computational Domain and Boundary Conditions

Schematics of two-dimensional compression corner is shown in **Fig. 3**. Flow conditions

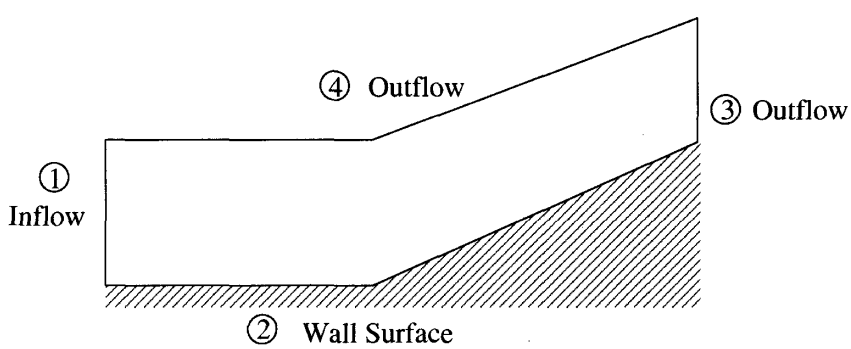

Fig. 3 Computational model and domain for shock wave-boundary layer interaction problem

are shown in **Table 2**. In case 1 thropugh case 3 shock Mach number, ramp angle, initial pressure and temperature in front of incident shock wave are same each other. Two types of flow conditions of chemically frozen and chemically non-equilibrium are assumed. In the chemically reacting flows fully catalytic wall condition (FCW) and non catalytic wall condition (NCW) are assumed. From case 4 through case 6 has same condition on shock Mach number and ramp angle, downstream temperature as case 1 through 3. However, initial pressure is lower compared with that of case 1 through case 3. Species concentrations of air can be approximately set as $c_{\mathrm{N}} = c_{\mathrm{O}} = c_{\mathrm{NO}} = 0$, $c_{\mathrm{N_2}} = 0.788$, $c_{\mathrm{O_2}} = 0.222$. Dissociation at downstream is neglected because degree of dissociation is small.

Table 2 Flow Conditions

	p_1 [Torr]	T_1 [K]	M_s	θ_w [deg]	Re [1/m]	Flow	Catalysis
case 1	50	2,000	5	30	8.3×10^6	Reacting	NCW
case 2	50	2,000	5	30	8.3×10^6	Reacting	FCW
case 3	50	2,000	5	30	8.3×10^6	Frozen	NCW
case 4	20	2,000	5	30	3.4×10^6	Reacting	NCW
case 5	20	2,000	5	30	3.4×10^6	Reacting	FCW
case 6	20	2,000	5	30	3.4×10^6	Frozen	NCW

2.4 Initial Condition and Computational Grid

In the present study, incident shock wave is generated 10 mm in front of the corner as initial condition. Conservation equations is solved behind shock wave with chemical reaction to give accurate condition. So, initial condition is obtained by solving steady one-dimensional inviscid conservation equations derived from two-dimensional conservation equations by classical four-stage Runge-Kutta method. The results are shown in **Fig. 4** $\sim$ **Fig. 5**. Temperature and density distributions behind incident shock wave are shown in **Fig. 4** and **Fig. 6**, and mole fraction distributions are shown in **Fig. 5** and **Fig. 7**. Chemical equilibrium state is established about 30 mm behind shock wave in the case of $p_1 = 50$ Torr about 110 mm behind incident shock wave in the case of $p_1 = 20$ Torr. Degrees of dissociation of the case of $p_1 = 20$ Torr is larger than that of the case of $p_1 = 50$ Torr at a point, where chemical equilibrium is established.

For boundary conditions, zero derivatives of physical variables are assumed at boundary of upstream and downstream of incident shock wave and at upper boundary. At the wall boundary, zero derivative of pressure, non-slip, constant wall temperature($T_w = T_1$) are assumed. FCW(Fully Catalytic Wall, k_w=∞) or NCW(Non Catalytic Wall, $k_w = 0$) conditions are imposed as species condition on the wall. However, it is suspicious that model of transport properties can describe phenomena adequately in the shock wave-boundary layer interaction[19]. Therefore, it is supposed that atoms are fully recombined at the fully catalytic wall to estimate maximum heating for safe design of the vehicles.

$$c_{s_w} = c_{s_1} \quad : \text{FCW Condition}$$
$$\left(\frac{\partial c_s}{\partial \eta}\right)_w = 0 \quad : \text{NCW Condition}$$

Computational grid for a ramp model is shown in **Fig. 8**. 600 grid points are distributed along x-direction, and 161 grid points are distributed along y-direction. Minimum grid spacing at the wall is 2.0×10^{-5} m.

3. Results and Discussion

Typical shock reflection patterns of the whole flow regions with and without chemical reactions are shown in **Fig. 9** and **Fig. 10**. Shock wave reflection pattern is DMR(Double Mach Reflection). It is observed shock wave patterns are different with each other. The distance between reflected shock wave and the wall is shorter than that of chemically frozen flow. Which is due to energy absorption by chemical reaction. Slip streams from triple point and intersection point of primary separation shock wave and reattachment shock wave of shock waves are clearly observed in **Fig. 10**.

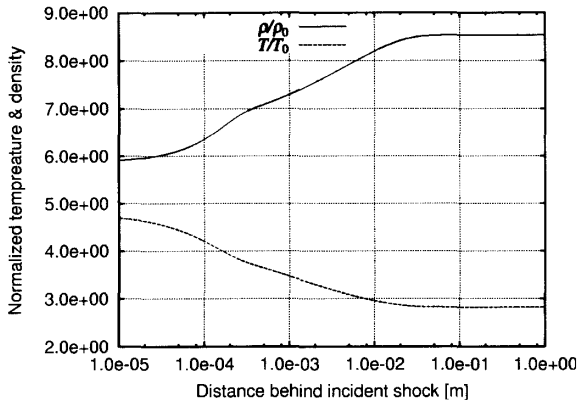

Fig. 4 Variation of temperature and density behind normal shock wave (p_1 = 50 Torr, T_1 = 2,000 K, $M_s = 5$)

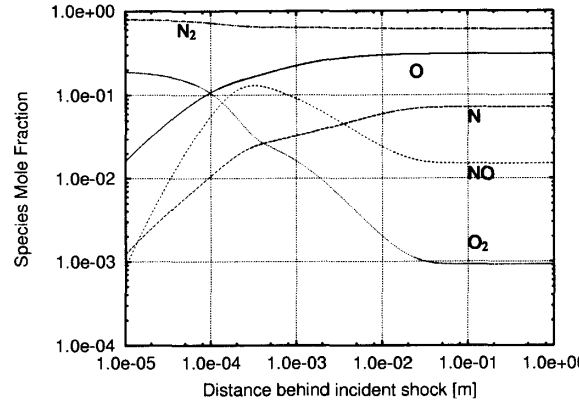

Fig. 5 Variation of mole fraction of each chemical species behind normal shock wave (p_1 = 50 Torr, T_1 = 2,000 K, $M_s = 5$)

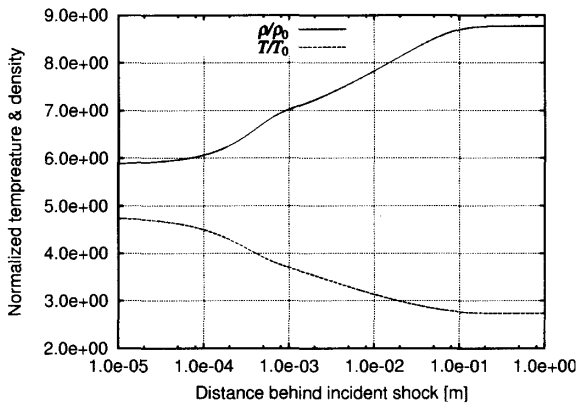

Fig. 6 Variation of temperature and density behind normal shock wave (p_1 = 20 Torr, T_1 = 2,000 K, $M_s = 5$)

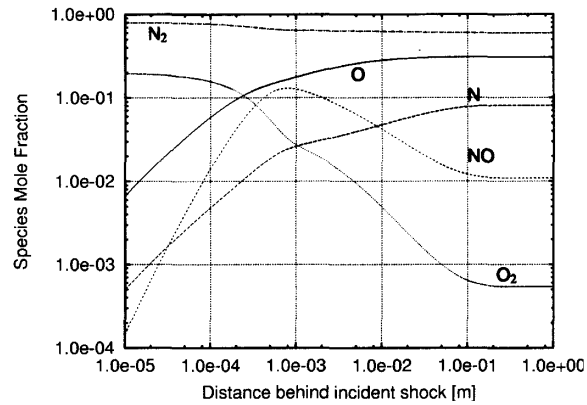

Fig. 7 Variation of mole fraction of each chemical species behind normal shock wave (p_1 = 20 Torr, T_1 = 2,000 K, $M_s = 5$)

Temperature contours near the corner are shown in **Fig. 11** ~ **Fig. 16** for cases (1) through (6).

Separation shock wave, reattachment shock wave and expansion waves are clearly captured by the present calculation. It is observed that angle of separation shock wave to the wall is larger in **Fig. 13** than that in **Fig. 11** and **Fig. 12** because dissociation of molecular species absorb energy. Same tendency is observed in cases (4) through (6) as shown in **Fig. 14**, **Fig. 15** and **Fig. 16**.

Instantaneous stream lines are shown **Fig. 17** ~ **Fig. 22**. Secondary separation is observed in primary separation in all cases of p_1= 50 Torr as shown in **Fig. 17**, **Fig. 18** and **Fig. 19**. However it is not observed in all cases of p_1= 20 Torr as shown in **Fig. 20**, **Fig. 21** and **Fig. 22**.

Shear stress distributions are shown in **Fig. 23** ~ **Fig. 26**. Separation point, reattachment point is clearly observed in **Fig. 24** and **Fig. 26**. Separation length, separation point and reattachment point are tabulated in **Table 3**.

The primary separation lengths of chemically reacting flows of FCW and NCW are

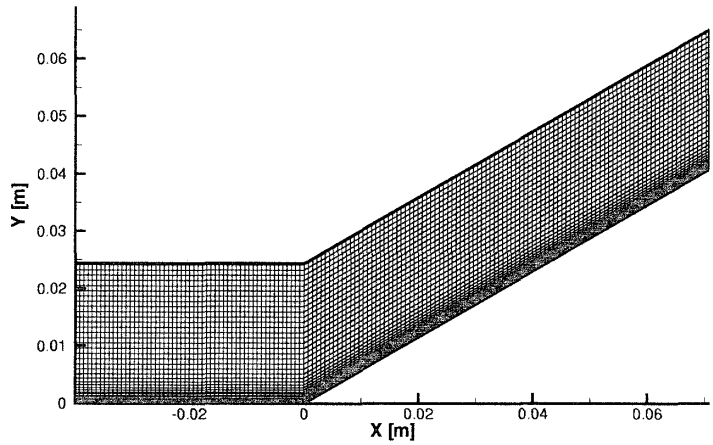

Fig. 8 Computational grid, 600×161 (every fourth grid lines are shown)

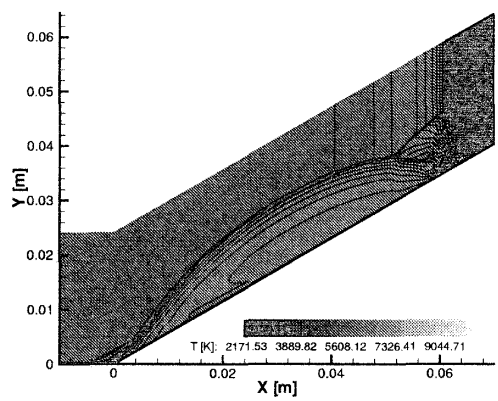

Fig. 9 Instantaneous temperature contours (case 1)

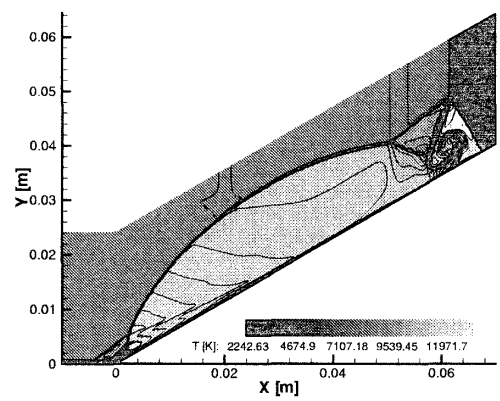

Fig. 10 Instantaneous temperature contours (case 3)

Table 3 Separation point, reattachment point and separation length

	x_{s1} [mm]	x_{r1} [mm]	L_p [mm]	x_{s2} [mm]	x_{r2} [mm]	L_s [mm]
case 1	-4.1	1.9	6.0	-0.8	-1.5	0.7
case 2	-4.0	2.0	6.0	-0.8	-1.4	0.6
case 3	-4.8	3.0	7.8	-0.9	-1.9	2.0
case 4	-4.0	2.4	6.4	-	-	-
case 5	-4.0	2.4	6.4	-	-	-
case 6	-4.4	3.4	7.8	-	-	-

smaller than that of chemically frozen flow because the angles of separation shock wave in chemically reacting flows are smaller due to dissociation of molecules than those in chemically frozen flows.

Surface heat flux distributions are shown in **Fig. 27** ~ **Fig. 30**. Large amount of surface heating is observed near the primary reattachment point, R_1. Local peak of surface heating

is also observed near the secondary reattachment point. At $p_1 = 50$ Torr peak heating at reattachment point of FCW (case 2) is three times larger than that of NCW (case 1). Peak heating at reattachment point of chemically frozen flow (case 3) is 1.5 times larger than that of NCW (case 2). Almost same tendency is observed at $p_1 = 20$ Torr. At $p_1 = 20$ Torr wall catalytic conditions for cases 4, 5 and 6 are NCW, FCW and chemically frozen respectively.

Surface pressure distributions are shown in **Fig. 31** $\sim$ **Fig. 34**. Large amount of surface pressure is observed near the primary reattachment point. local peak of surface pressure is also observed near the secondary reattachment point. At $p_1 = 50$ Torr peak pressures at reattachment points in case 1 through 3 are about 4.0 time of upstream undisturbed level. Significant difference is not observed in surface peak pressure among chemically reacting flow with FCW and NCW and chemically frozen flow. Almost same tendency is observed at $p_1 = 20$ Torr.

Ratio of local surface pressure peak with surface pressure at further upstream from upstream influence region is tabulated in **Table 4**. Ratio of local surface heat flux peak with surface heat flux at further upstream from upstream influence region is also tabulated in **Table 4**. Degree of dissociation might plays some roles on shock wave-boundary layer

Table 4 Ratio of surface pressure and heat flux

	p_{p1}/p_u	q_{p1}/q_u
case 1	2.3	4.0
case 2	2.3	4.0
case 3	3.0	4.0
case 4	2.3	4.5
case 5	2.3	4.5
case 6	2.3	4.0

interaction. p_{p1}/p_u is larger in case 4 and case 5 than case 1 and case 2. q_{p1}/q_u is larger in case 3 than case 6, and it is same in case 1 and case 2 as case 4 and case 5. Only two case of p_1 is investigated in the present study, so further investigation might have to be done to research effects of p_1.

4. Conclusions

Shock wave-boundary layer interaction in high enthalpy flow is numerically simulated assuming thermal equilibrium and chemical nonequilibrium condition. From the results from the present numerical simulation, effects of chemical nonequilibrium and downstream pressure in shock wave-boundary layer interaction can be observed. They are summarized as below.

1. The primary separation lengths of chemically reacting flows of FCW and NCW are smaller than that of chemically frozen flow because the angles of separation shock wave in chemically reacting flows are smaller due to dissociation of molecules than those in chemically frozen flows.

2. Large amount of surface heating is observed near the primary reattachment point, R_1. Local peak of surface heating is also observed near the secondary reattachment point. At $p_1 = 50$ Torr peak heating at reattachment point of FCW (case 1) is three times

larger than that of NCW (case 2). Peak heating at reattachment point of chemically frozen flow is 1.5 times larger than that of NCW (case 2). Almost same tendency is observed at $p_1 = 20$ Torr.

3. Large amount of surface pressure is observed near the primary reattachment point. local peak of surface pressure is also observed near the secondary reattachment point. At $p_1 = 50$ Torr peak pressures at reattachment points in case 1 through 3 are about 4.0 time of upstream undisturbed level. Significant difference is not observed in surface peak pressure among chemically reacting flow with FCW and NCW and chemically frozen flow. Almost same tendency is observed at $p_1 = 20$ Torr.

References

1) J. Olejniczak, G. V. Candler, M. J. Wright, I. Leyva, and H. G. Hornung: Experimental and Computational Study of High Enthalpy Double-Wedge Flows, Journal of Thermophysics and Heat Transfer, Vol.13 No. 4, pp.431-440, 1999
2) M. J. Wright, J. Olejniczak, G. V. Candler, T. D. Magruder, and A. J. Smits: Numerical and Experimental Investigation of Double-Cone Shock Interactions, AIAA Journal, Vol.38 No. 4, pp.2268–2276, 2000
3) J. Olejniczak, M. J. Wright, and G. V. Candler: Numerical Study of Inviscid Shock Interactions on Double-Wedge Geometries, Jounal of Fluid Mechanics, Vol.352 pp.1-25, 1997
4) J. Davis and B. Sturtevant: High-Enthalpy Shock/Boundary-Layer Interaction on a Double Wedge : Real-Gas Effects on Separation Length, Proc. 22nd. International Symposium on Shock Waves, No. 0370, Imperial College, London, UK, 1999
5) A. Grumet, J. D. Anderson Jr, and M. J. Lewis: Numerical Study of the Effects of Wall Catalysis on Shock Wave/Boundary-Layer Interaction, Journal of Thermophysics and Heat Transfer, Vol.8 No. 1, pp.40-47, 1994
6) F. Grasso, M. Marini, G. Ranuzzi, S. Cuttica, and B. Chanetz: Shock-Wave/Turbulent Boundary-Layer Interactions in Nonequilibrium Flows, AIAA Journal, Vol.39 No. 1, pp.2131-2140, 2001
7) S. G. Mallinson, S. L. Gai, and N. R. Mudford: The Interaction of a Shock Wave with a Laminar Boundary Layer at a Compression Corner in High-Enthalpy Flows Including Real Gas Effects, Journal of Fluid Mechanics, Vol.342, pp.1-35, 1997
8) F. G. Blottner: Viscous Shock Layer at The Stagnation Point with Nonequilibrium Air Chemistry, AIAA Journal, Vol.7 No. 12, pp.2281-2288, 1969
9) J. M. Yos: Transport Properties of Nitrogen, Hydrogen, Oxygen, and Air to 30,000 K, Technical Memorandum, RAD-TM-63-7, AVCO-RAD, 1963
10) R. N. Gupta, J. M. Yos, R. A. Thompson, and K.-P. Lee: A Review of Reaction Rates and Thermodynamic and Transport Properties for 11-Species Air Model for Chemical and Thermal Nonequilibrium Calculation to 30,000 K, Reference Publication, 1232, NASA, 1989
11) W. W. Jones, and J. Boris: An Algorithm for Multispecies Diffusion Fluxes, Computers & Chemistry, Vol.5 No. 2-3, pp.139-146, 1981
12) C. F. Curtiss, and J. O. Hirschfelder: Transport Properties of Multicomponent Gas Mixture, Journal of Chemical Physics, Vol.17 No. 6, pp.550-555, 1949
13) J. H. Lee: Basic Governing Equations for the Flight Regimes of Aeroassisted Orbital Transfer Vehicles, In AIAA Paper, No.84-1729,1984.

14) P. A. Gnoffo, R. N. Gupta, and J. L. Shinn: Conservation Equations and Physical Models for Hypersonic Air Flows in Thermal and Chemical Nonequilibrium, TP-2867, NASA, 1989
15) Y. Wada, and M.-S. Liou: A Flux Splitting Scheme with High-Resolution and Robustness for Discontinuities, AIAA Paper, No.94-0083, 1994
16) B. Van Leer: Towards Ultimate Conservative Difference Scheme V. A Second-Order Sequel to Godunov's Method, Journal of Computational Physics, Vol.32, pp.101–136, 1979
17) W. K. Anderson, J. L. Thomas, and B. Van Leer: Comparison of Finite Volume Flux Vector Splitting for the Euler Equations, AIAA Journal, Vol.24 No. 9, pp.1453-1460, 1986
18) A. Jameson, W. Shmidt, and E. Turkel: Numerical Simulation of the Euler Equations by Finite Volume Method using Runge-Kutta Time Stepping Shemes, AIAA Paper, NO.81-1259, 1981
19) C. Park: Validation of CFD Codes for Real-Gas Regime, AIAA Paper, No.97-2530, 1997

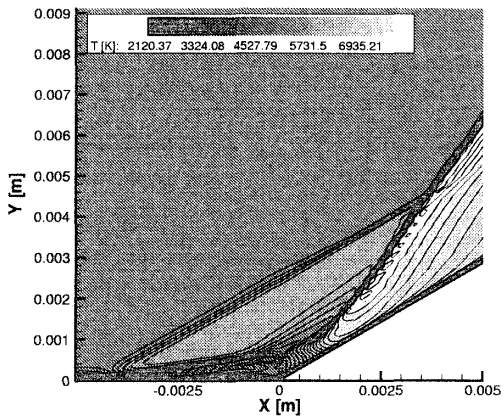

Fig. 11 Temperature contours near the corner (case 1)

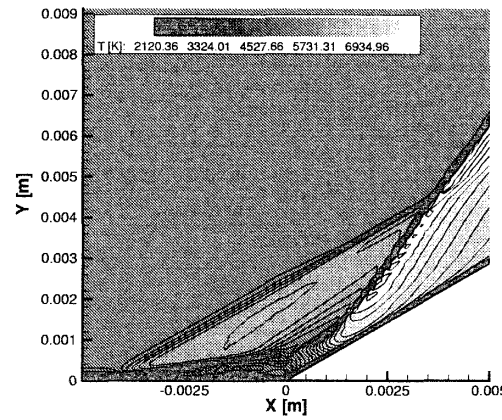

Fig. 12 Temperature contours near the corner (case 2)

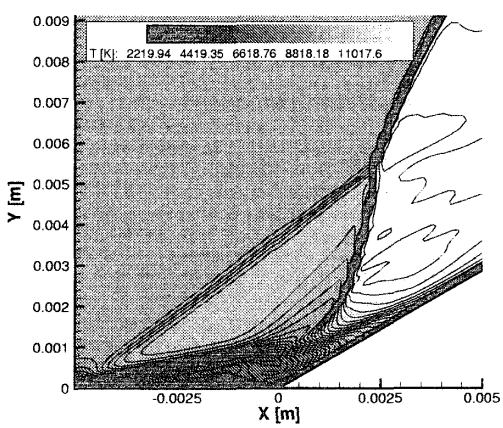

Fig. 13 Temperature contours near the corner (case 3)

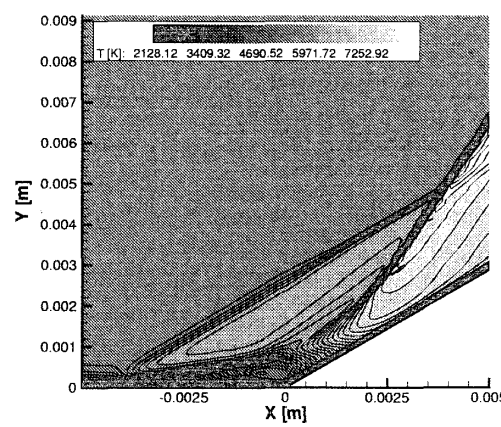

Fig. 14 Temperature contours near the corner (case 4)

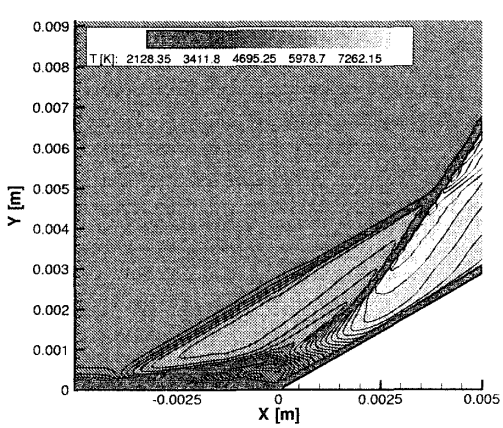

Fig. 15 Temperature contours near the corner (case 5)

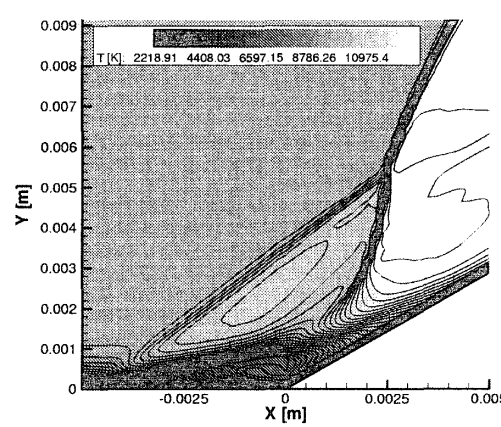

Fig. 16 Temperature contours near the corner (case 6)

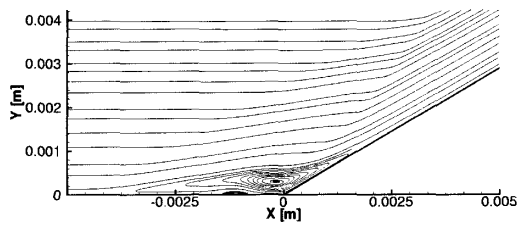

Fig. 17 Stream line trace near the corner (case 1)

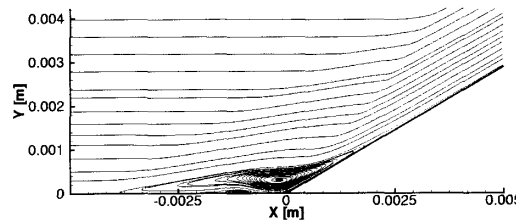

Fig. 18 Stream line trace near the corner (case 2)

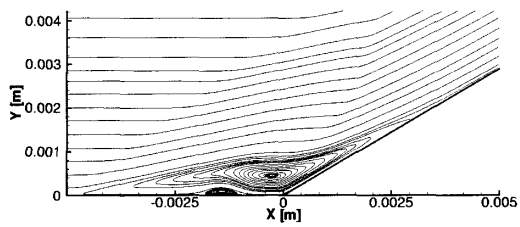

Fig. 19 Stream line trace near the corner (case 3)

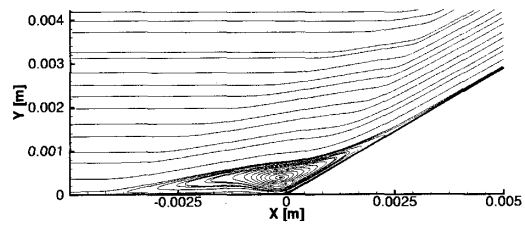

Fig. 20 Stream line trace naer the corner (case 4)

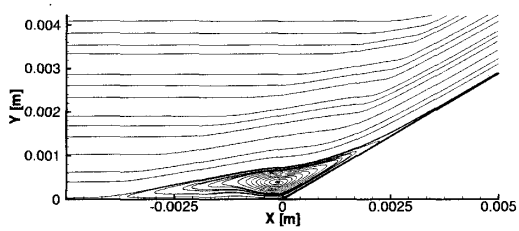

Fig. 21 Stream line trace near the corner (case 5)

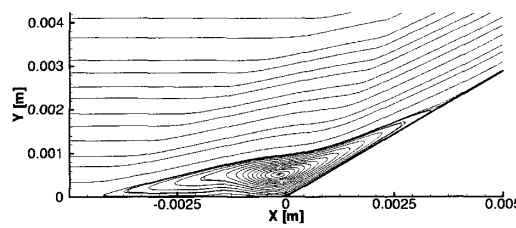

Fig. 22 Stream line trace near the corner (case 6)

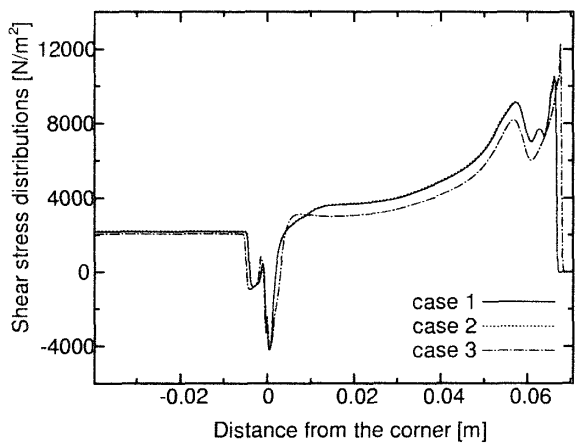

Fig. 23 Shear stress distributions (case 1 ~ case 3)

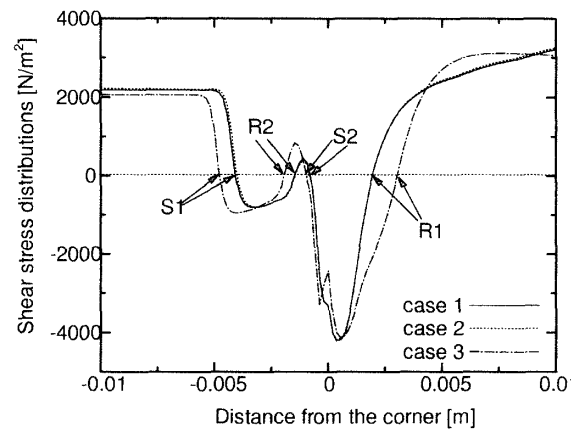

Fig. 24 Shear stress distributions near the corner (case 1 ~ case 3)

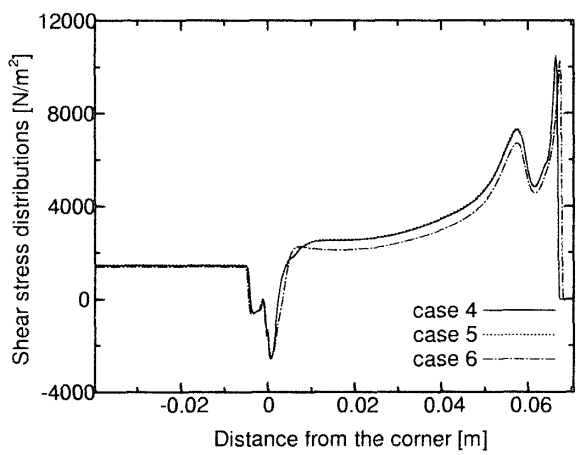

Fig. 25 Shear stress distributions (case 4 ~ case 6)

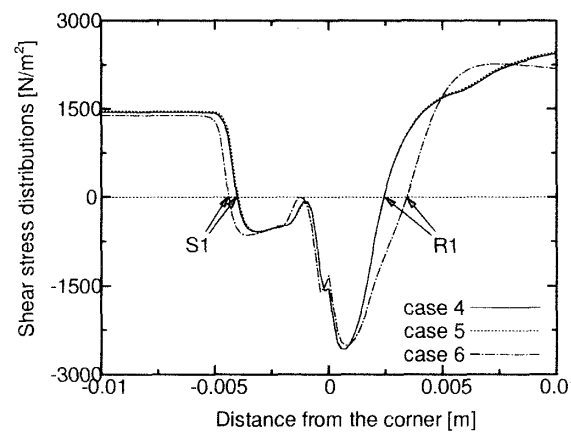

Fig. 26 Shear stress distributions near the corner (case 4 ~ case 6)

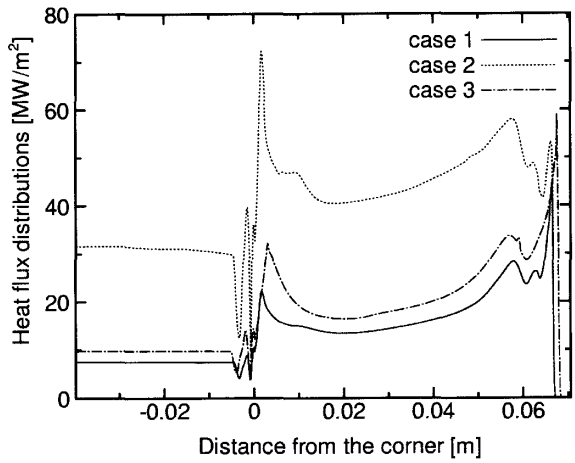

Fig. 27 Surface heat flux distributions (case 1 ~ case 3)

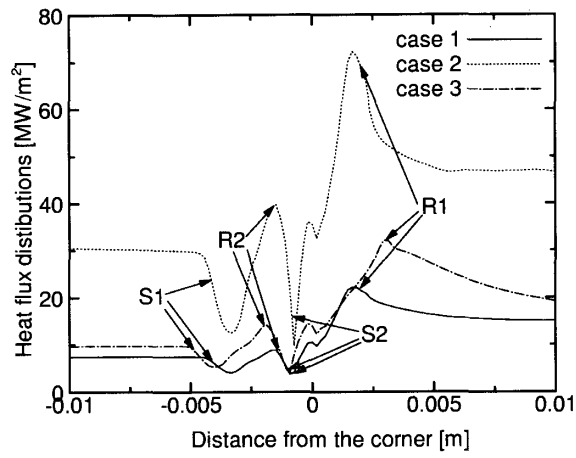

Fig. 28 Surface heat flux distributions near the corner (case 1 ~ case 3)

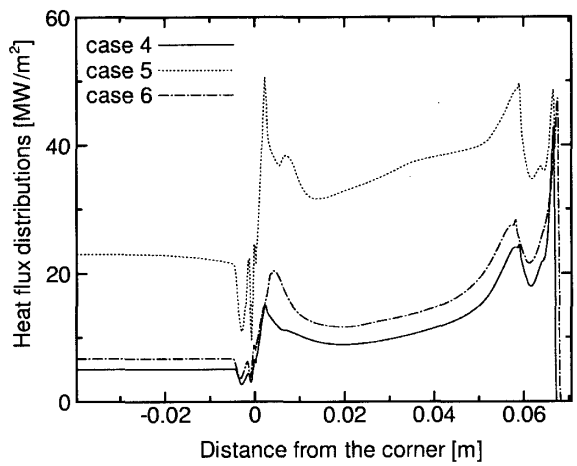

Fig. 29 Surface heat flux distributions (case 4 ~ case 6)

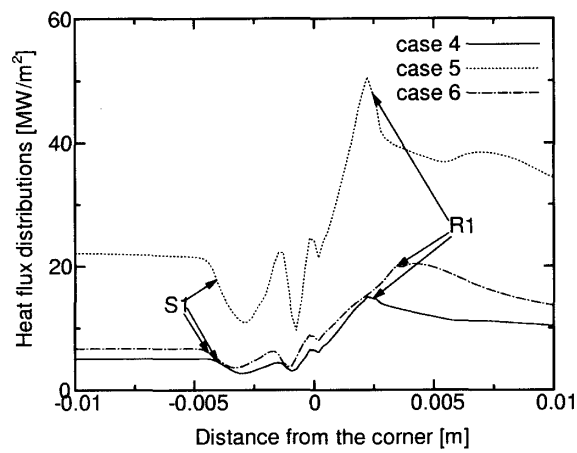

Fig. 30 Surface heat flux distributions near the corner (case 4 ~ case 6)

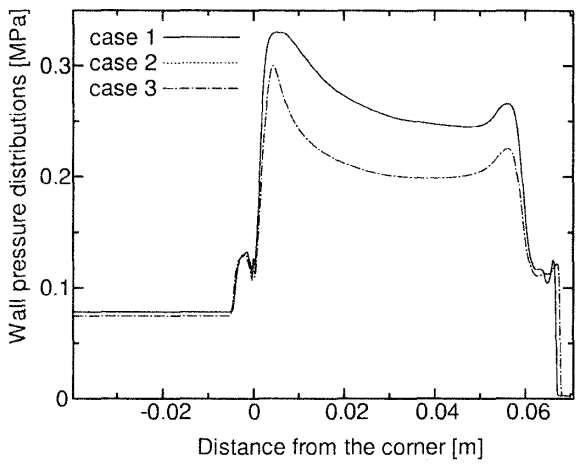

Fig. 31 Surface pressure distributions (case 1 $\sim$ case 3)

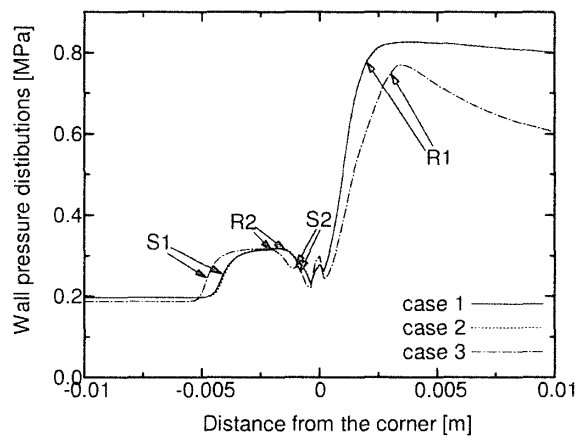

Fig. 32 Surface pressure distributions near the corner (case 1 $\sim$ case 3)

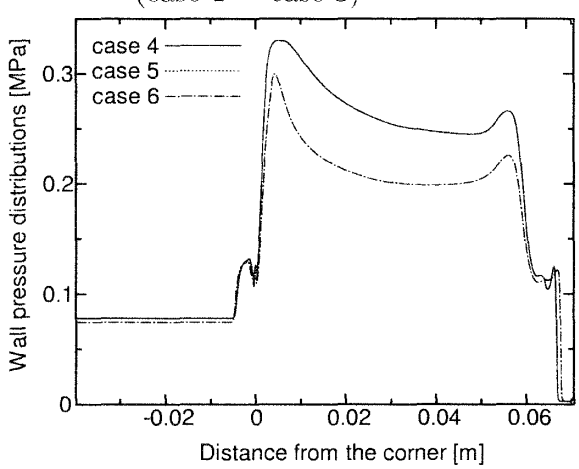

Fig. 33 Surface pressure distributions (case 4 $\sim$ case 6)

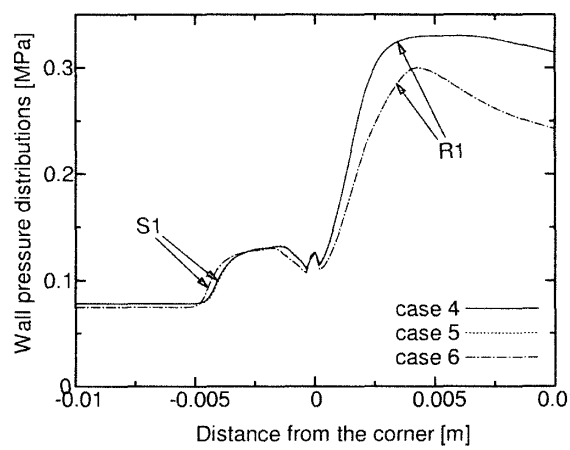

Fig. 34 Surface pressure distributions near the corner (case 4 $\sim$ case 6)